Highly efficient 3D first-arrival traveltime tomography by stochastic approximation

Mengyao Sun and Jie Zhang, University of Science and Technology of China; Mauricio Sacchi, University of Alberta*

Summary

Near-surface solutions often play a significant role in producing high quality subsurface images for land or shallow marine environments. First-arrival traveltime tomography is a common approach for solving the near-surface imaging problem. However, for 3D cases, the seismic surveys commonly deploy over ten thousands of sources combined with thousands of receivers, leading to millions of traveltime picks and therefore require time consuming computations. Consequently, conventional methods we employ now may suffer from large memory requirement and long computation time. We propose to improve the efficiency of traveltime tomography by introducing the theory of Stochastic Approximation (SA). Our approach is to derive near-surface models by employing only a small percentage of data in inversion following SA algorithm. We assess the efficiency of the method by a synthetic test and a real data application; the results show that the long-wavelength statics corrections calculated from the solution obtained by the new method is nearly identical to the one obtained by the conventional method. However, only less than 20% data is utilized in 3D tomography during the inversion. Both computational memory and time are significantly reduced.

Introduction

Computation cost is an inevitable issue that should be considered for geophysical imaging. Particularly for exploration industry today, more and more data have been acquired and data processing efficiency is becoming more challenging. Stochastic approximation (SA) (Nemirovski et al., 2009) is one of the efficient methods applied in geophysical imaging, such as Full Waveform Inversion (FWI) (Herrmann et al., 2011; Li et al., 2012). Our interest in this study is to reduce the computational cost of the 3D traveltime tomography (Zhang and Toköz, 1998) by applying SA. This study is especially meaningful for dealing with large 3D datasets.

The basic idea of SA is to solve a large optimization problem by sampling partial data randomly. Additionally, the sampling pattern at each iteration should be changed during the inversion. The final solution of SA is derived by a mathematical expectation, in which many inversions with different input data should be performed and it is not efficient. We therefore propose a fast way to handle the practical implementations and we demonstrate the accuracy and the efficiency by a synthetic test and a real data application. In the following, we shall call the new method Fast Stochastic Approximation Tomography (FSAT), and the result obtained by the conventional tomography method with full data included is named standard result.

Theory

First-arrival traveltime tomography is currently a standard approach for imaging near surface structures and it has been tremendously improved over the yeas. The following equation shows the objective function of traveltime tomography

$$\Phi(\boldsymbol{m},\boldsymbol{d}) = \|\boldsymbol{d} - G(\boldsymbol{m})\|^2 + \lambda\|\boldsymbol{R}\boldsymbol{m}\|^2, \qquad (1)$$

here, $\boldsymbol{m}$ is the model slowness, $\boldsymbol{d}$ represents the observed traveltimes, $G(\boldsymbol{m})$ contains the calculated traveltime, λ is a constant parameter for balancing the data misfit and model regularization and $\boldsymbol{R}$ is the regularization operator. The minimization of equation (1) is often carried out via the Gauss-Newton method where in each iteration one solves for slowness perturbations via the conjugate gradient (CG) (Hestenes et al., 1952) method. The final nonlinear optimization process to retrieve the slowness can be written as follows

$$\boldsymbol{m}_{k+1} = \boldsymbol{m}_k + \Delta\boldsymbol{m}\,, \qquad (2)$$

where the slowness perturbations are computed by solving the following equation via the CG method

$$(\boldsymbol{A}^T\boldsymbol{A} + \lambda\boldsymbol{R}^T\boldsymbol{R})\Delta\boldsymbol{m} = \boldsymbol{A}^T\big(\boldsymbol{d} - G(\boldsymbol{m}_k)\big) - \lambda\boldsymbol{R}^T\boldsymbol{R}\boldsymbol{m}_k$$

The matrix $\boldsymbol{A}$ is the Jacobian or Sensitivity matrix of the traveltime tomography problem. The algorithm proceeds until a convergence criterion is satisfied or a maximum iteration number is reached.

The idea of SA is to define K data sets by randomly extracting L observations (picks) from the original data and solve the following inverse problem

$$\boldsymbol{m}^j = \underset{\boldsymbol{m}}{\operatorname{argmin}}\,\Phi(\boldsymbol{m},\boldsymbol{\xi}^j)\,, j = 1, P. \qquad (3)$$

Where $\boldsymbol{\xi}^j$ is the $L \times 1$ j^{th} vector of picks randomly extracted from $\boldsymbol{d}$. The traveltime picks are extracted using a uniform random number integer $u \in [1, N]$ distribution with no repetition of picks. Additionally, one should pick a new $\boldsymbol{\xi}$ vector for each iteration during the inversion. Then the final estimator of the tomographic model can be computed as

$$\boldsymbol{m}_{SA} = \frac{1}{P}\sum_{j=1}^{P} \boldsymbol{m}_{SA}^{j}, \quad (4)$$

The FSAT is proposed for expecting to speed up the tomographic problem and maintaining the accuracy of the solution. The main idea of FSAT is to make the parameter P in equation (4) be equal to 1. Because we find that for first-arrival traveltime tomography, the inversion result is satisfying if the size of subset $\boldsymbol{\xi}$ is appropriate even though P is equal to 1. Therefore, only one inversion process needs to be performed and the solution is described as follows

$$\boldsymbol{m}_{FSA} = \boldsymbol{m}_{SA}^{1}, \quad (5)$$

The following provides the algorithm of FSAT.

1: $\boldsymbol{m}_1 = \boldsymbol{m}_{ini}$
2: $\boldsymbol{do}\ k = 1, itx$
3: $(\boldsymbol{A}_k^T\boldsymbol{A}_k + \lambda\boldsymbol{R}^T\boldsymbol{R})\Delta\boldsymbol{m} = \boldsymbol{A}_k^T\big(\boldsymbol{d}(\boldsymbol{\xi}_k) - G(\boldsymbol{m}_k, \boldsymbol{\xi}_k)\big) - \tau\boldsymbol{R}^T\boldsymbol{R}(\boldsymbol{m}_k)$
4: $\boldsymbol{m}_{k+1} = \boldsymbol{m}_k + \Delta\boldsymbol{m}$
5: $\boldsymbol{enddo}$
6: $\boldsymbol{m}_{FSA} = \boldsymbol{m}_{itx+1}$

The vector $\boldsymbol{m}_{ini}$ is the initial model, itx is the max iteration number and $\boldsymbol{A}_k$ is the sensitivity matrix at iteration k.

Synthetic test

Figure 1a shows the true model of a synthetic test. The model consists of 267(X) × 258(Y) × 28(Z) cells. The cell sizes in X, Y, and Z coordinate are 68 m, 68 m, and 34 m, respectively. The coordinate ranges of the three dimensions are 185,402~203,490 m (X), 1,051,657~1,069,133 m (Y), and -1,472~-554 m (Z), respectively. The acquisition geometry is also shown in Figure 1a, the red dots represent shots and the green dots represent receivers. The shot distribution and the receivers for a shot are also displayed in Figure 2a (Red dots are shots and yellow dots are receivers). There are 1,200 shots and 3,900 unique receivers in total. The max number of receivers for a shot is 600 and the max offset is 5,699 m in this case. We generate the synthetic traveltime data by performing 3D raytracing based on eikonal equation. We build an initial model by employing the analytical formula for the average refraction traveltimes. The conventional first-arrival traveltime tomography employing all of the data during inversion is performed for presenting a standard result to evaluate the performance of FSAT. The total iteration number for the conventional method is set 25. For FSAT, we extract 200 shots randomly for the inversion, the extracted shots are renewed at each iteration. We show three data examples of the extraction patterns in Figure 2b, c, and d, as the input shots of three iterations during the inversion. The max iteration number of FSAT is also set 25. Figure 1b, e, and h are the velocity profiles of the true model at different dimensions (Z=-1262 m, Y=1,055,329 m, and X= 193,834 m). The corresponding velocity profiles of the standard result and the FSAT result are shown in Figure 1c, f, i, and Figure 1d, g, j, respectively. We observe that the result obtained by the conventional method and FSAT are almost identical.

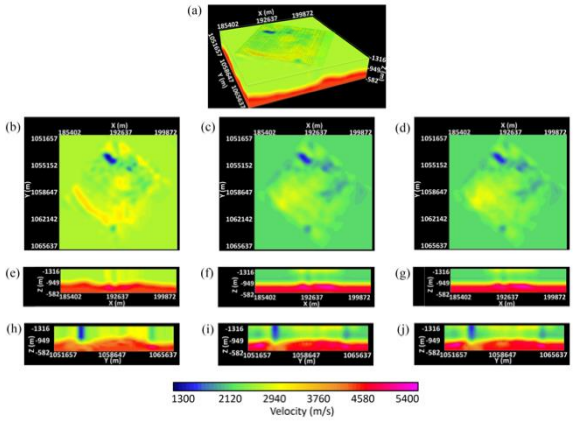

Figure 1: Velocity models of the synthetic test. (a) The true model and the acquisition geometry. (b), (c), and (d) The velocity profiles of the true model, standard result, and the FSAT result at Z=-1,262 m. (e), (f), and (g) The velocity profiles of the true model, the standard result, and the FSAT result at Y=1,055,329 m. (h), (i), and (j) The velocity profiles of the true model, the standard result, and the FSAT result at X= 193,834 m.

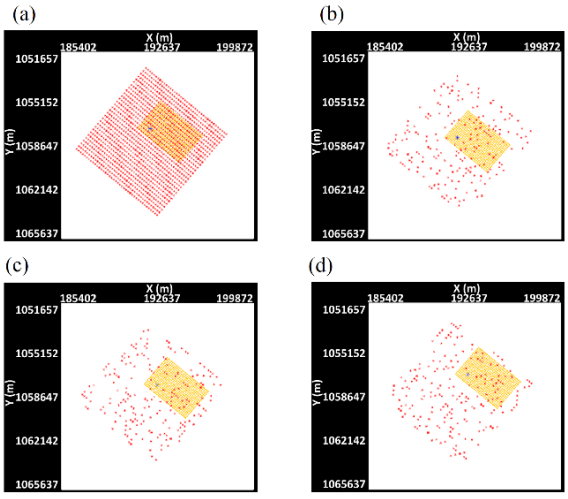

Figure 2: (a) The acquisition geometry of the synthetic test. (b), (c), and (d) Three examples of the selected input shots for FSAT during the inversion.

To further study the performance of FSAT, we calculate the shot and receiver long-wavelength statics with the standard model result and the FSAT result, as shown in Figure 3a and b, respectively. The difference between the long-wavelength statics calculated by the two different models is also displayed in Figure 3c. We observe that their difference is small and less than 2 sampling points. There should not be much difference in the subsequent data processing. That means, FSAT provides an almost identical result as the conventional method, however, with only 1/6 data. The estimated memory usage for the conventional inversion method is about 230 MB, however, only 100 MB for FSAT. We also record the computational time cost for the conventional method and FSAT in a same running environment, they are 126 min and 42 min, respectively.

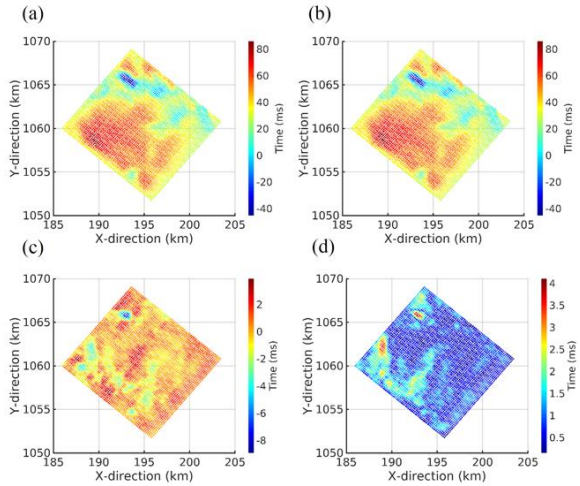

Figure 3: The long-wavelength shot and receiver statics comparison of the synthetic test. (a) The statics calculated by the standard model result. (b) The statics calculated by the FSAT result. (c) The difference between (a) and (b). (d) The RMS statics error of the twenty tests.

Another important issue we should discuss is the stability of FSAT. One may concern that if a different random extracted pattern would affect the final result significantly. We investigate this problem by running 20 times FSAT with a different data extraction pattern every time. We calculate the RMS error of long-wavelength statics for each shot and each receiver via

$$\boldsymbol{\sigma} = \sqrt{\frac{1}{Q}\sum_{q=1}^{Q}(\boldsymbol{s}_q^{FSA} - \boldsymbol{s}^*)^2}. \quad (6)$$

and present the result in Figure 3d. The result shows a satisfying stability of the FSAT method with the RMS error always in about 1~2 samples. The parameter $\boldsymbol{\sigma}$ represents the RMS error of the shot and receiver long-wavelength statics, Q is the number of times that FSAT is performed. Similarly, $\boldsymbol{s}_q^{FSA}$ represents the long-wavelength statics of q^{th} test and it is derived by FSAT method. The vector $\boldsymbol{s}^*$ is the long-wavelength statics derived by the conventional method that uses all the data.

Real data application

We further apply FSAT to a real dataset. Figure 4a shows the initial model built by the same analytical method as the synthetic test. The model size and the grid size of this real data is the same as the synthetic model because we design the synthetic model according to this real data. The acquisition geometry is shown in Figure 4a. The red dots represent shots and the green dots represent receivers. The total shot number and unique receiver number are 1,041 and 4,150, respectively. The max receiver number for one shot is 1,163 and the max offset is 4,084 m. Figure 5a also displays the shot distributions and the receivers for one shot (in yellow). Figure 4b shows the rugged topography of this case and it is different from the synthetic test. The first arrivals are picked manually. We perform the same procedures for this real data. For the conventional method, 25 iterations are set to execute. For FSAT, we also extract 200 shots and update the extraction pattern at each iteration. Figure 5b, c, and d show three examples of the data extraction pattern during the inversion. The max iteration number is 25 as well. Figure 4c, e, and g are the velocity profiles of the standard result at different dimensions (Z=-928 m, Y=1,061,177 m, and X= 192,406 m). The corresponding velocity profiles of FSAT result are displayed in Figure 4d, f, and h. We also observe good similarity between the standard result and the FSAT result.

Similarly, for further evaluating the performance of FSAT on the real case, we calculate the long-wavelength shot and receiver statics with the standard model result and the FSAT result and show them in Figure 6a and b. The difference between that in Figure 6a and b is also displayed in Figure 6c. We observe that the difference range in this real case is also 1~2 time samples. There should not be much difference in the subsequent data processing. The stability of this case is also investigated by performing 20 times FSAT. The RMS statics error is shown in Figure 6d. The result is consistent with the synthetic test and it implies that FSAT could provide a satisfying and stable result and save both memory and computational time cost. In this case, the estimated memory usage for the conventional method is about 300 MB, however, 120 MB is required for FSAT. On the other hand, the time cost of the conventional method and FSAT is 133 min and 53 min, respectively.

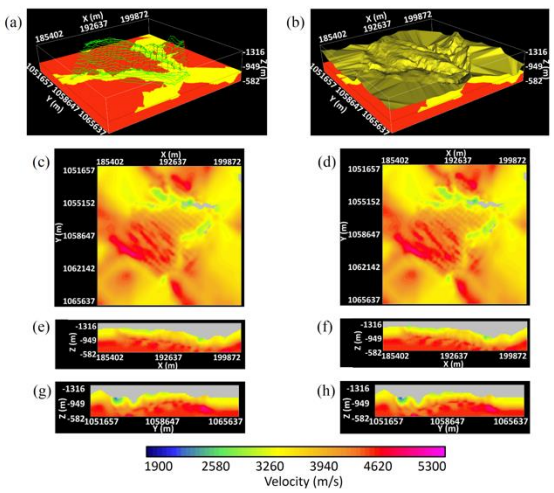

Figure 4: Velocity models of the real data application. (a) The initial model and the acquisition geometry. (b) The topography of the real data. (c) and (d) The velocity profiles of the standard result and the FSAT result at Z=-928 m. (e) and (f) The velocity profiles of the standard result and the FSAT result at Y=1,061,177 m. (g) and (h) The velocity profiles of the standard result and the FSAT result at X= 192,406 m.

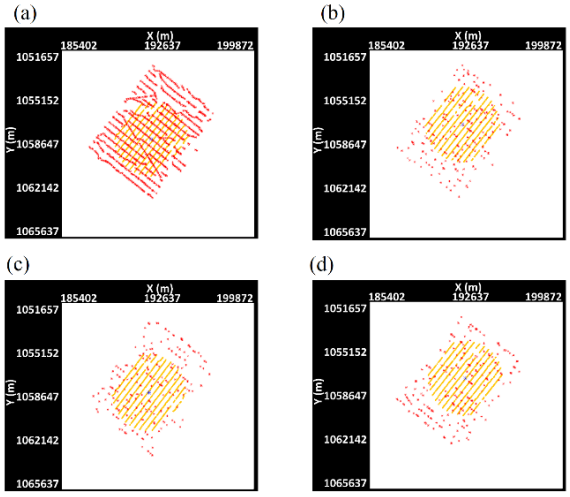

Figure 5: (a) The acquisition geometry of the real data application. (b), (c), and (d) Three examples of the selected input shots for FSAT during the inversion.

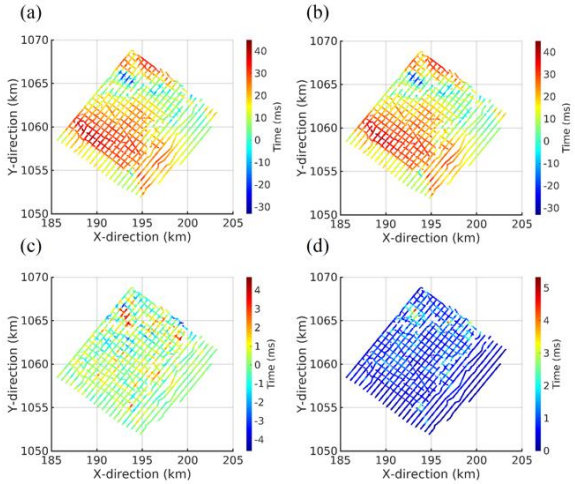

Figure 6: The shot and receiver long-wavelength statics comparison of the real data application. (a) The statics calculated by the standard model result. (b) The statics calculated by the FSAT result. (c) The difference between (a) and (b). (d) The RMS statics error of the twenty tests.

Conclusions

We propose a highly efficient method called FSAT by developing the mathematical theory SA for 3D first-arrival traveltime tomography. The method is implemented by employing a small part of data during the inversion. A synthetic test and real data example demonstrate that FSAT obtains an almost identical statics solution as the conventional method and saves both memory and running time during the inversion.

Acknowledgements

We gratefully acknowledge the financial support of the National Natural Science Foundation of China (Grant No. 41674120) and the China Scholarship Council (CSC). The support and enthusiasm of Signal Analysis & Imaging Group (SAIG) is gratefully acknowledged. We also appreciate GeoTomo for providing TomoPlus software package to conduct this work.

References

Herrmann, F. J., X. Li, A. Y. Aravkin and T. Van Leeuwen, 2011, September. A modified, sparsity-promoting, Gauss-Newton algorithm for seismic waveform inversion: In SPIE Optical Engineering+ Applications, International Society for Optics and Photonics, 81380V-81380V.

Hestenes, M.R. and E. Stiefel, 1952. Methods of conjugate gradients for solving linear systems, **49**, 1, NBS.

Li, X., A. Y. Aravkin, T. Van Leeuwen and F. J. Herrmann, 2012, Fast randomized full-waveform inversion with compressive sensing: Geophysics, **77**, no. 3, A13-A17.

Nemirovski, A., Juditsky A., Lan G. and Shapiro A., 2009, Robust stochastic approximation approach to stochastic programming: SIAM Journal on Optimization, **19**, no. 4, 1574– 1609.

Zhang J. and M. N. Toksöz, 1998, Nonlinear refraction traveltime tomography: Geophysics, **63**, no. 5, 1726-1737.